Celest Mech Dyn Astr (2013) 115:35–57
DOI 10.1007/s10569-012-9450-y

ORIGINAL ARTICLE

Analytical solutions for J_2-perturbed unbounded equatorial orbits

Vladimir Martinusi · Pini Gurfil

Received: 30 March 2012 / Revised: 29 August 2012 / Accepted: 11 October 2012 /
Published online: 3 November 2012
© Springer Science+Business Media Dordrecht 2012

Abstract While solutions for bounded orbits about oblate spheroidal planets have been presented before, similar solutions for unbounded motion are scarce. This paper develops solutions for unbounded motion in the equatorial plane of an oblate spheroidal planet, while taking into account only the J_2 harmonic in the gravitational potential. Two cases are distinguished: A pseudo-parabolic motion, obtained for zero total specific energy, and a pseudo-hyperbolic motion, characterized by positive total specific energy. The solutions to the equations of motion are expressed using elliptic integrals. The pseudo-parabolic motion unveils a new orbit, termed herein the fish orbit, which has not been observed thus far in the perturbed two-body problem. The pseudo-hyperbolic solutions show that significant differences exist between the Keplerian flyby and the flyby performed under the the J_2 zonal harmonic. Numerical simulations are used to quantify these differences.

Keywords Perturbed two-body problem · Zonal harmonics · Analytical methods · Unbounded orbits

1 Introduction

The problem of the motion of a satellite about an oblate planet, while considering only the J_2 term in the gravitational potential, is also known as "The Main Problem" in artificial satellite theory (Deprit and Rom 1970). Generally, the problem is not integrable, except for equatorial orbits, and may even theoretically exhibit chaotic behavior under some specific initial conditions (Celletti and Negrini 1995; Irigoyen and Simo 1993). Since the J_2 zonal harmonic is the main perturbation affecting low-orbiting satellites, several methods to solve this problem

V. Martinusi · P. Gurfil (✉)
Distributed Space Systems Lab, Faculty of Aerospace Engineering, Haifa, Israel
e-mail: pgurfil@technion.ac.il

V. Martinusi
e-mail: vladmartinus@gmail.com

were developed, starting with the celebrated Brouwer and Kozai theories (Brouwer 1959; Kozai 1962).

Integrable solutions for truncated zonal potentials have been thoroughly studied using various approximations, the most notable of which are Vinti's potential (Vinti 1960), Cid's radial intermediary (Cid and Lahulla 1969; Deprit and Ferrer 1989, 1987; Coppola and Palacián 1994), and the two fixed centers model (Beletskii 2001).

However, only few efforts to study unbounded orbits under the effect of approximated zonal potentials can be found in the literature. Lang (1968) and O'Mathuna (1970) offered prolate-spheroidal solutions for open orbits while considering Vinti's approximate potential (Vinti 1959, 1961a,b,c). Whitman and Matese (1985) introduced generalized Lagrangian orbital elements to describe the motion in a central force field by means of variational equations, which also hold for open orbits.

The present paper offers analytical solutions for unbounded motion in the equatorial plane of a planet while considering only the J_2 zonal harmonic. The derivation of these solutions is possible mainly because in this particular situation, the problem is super-integrable in the sense of Liouville, since it admits four known independent first integrals of motion, given by the specific angular momentum vector and the specific total energy. Thus, since the critical points of the radial distance function are obtained by solving a cubic equation, the general solution may be expressed with the help of elliptic integrals (Jezewski 1983; Martinusi and Gurfil 2011).

The problem of unbounded orbits is solved for two situations: (i) the velocity vanishes at infinity (the zero specific energy case) and (ii) the magnitude of the velocity approaches asymptotically a constant positive value (the positive specific energy case).

The problem is solved in terms of polar coordinates in the plane of motion, with respect to a fixed reference axis. Vectorial orbital elements are defined, namely the specific angular momentum vector and a replica of the pericenter (or the eccentricity) vector. The vectorial solution is expressed with respect to these elements, which can be determined at the initial moment of time as explicit functions of the initial conditions.

In particular, a new orbit is revealed in the case of zero-energy unbounded motion, which is named *the fish orbit* due to its unusual shape. To the knowledge of the Authors, it is the first time that such an orbit is determined in the perturbed two-body problem. The orbit has some unusual geometric properties, which are analyzed in the current work. This orbit may be viewed as a natural continuation of the precessing orbits in the negative-energy case.

The practical applications of the present approach are related to the positive total energy case, where it is shown that the flyby parameters are significantly changed if the J_2 zonal harmonic is taken into consideration. It is proven that a significant deflection angle difference, as well as a pericenter shift, may exist in the J_2 flyby vis-à-vis the Keplerian flyby.

2 Mathematical preliminaries

When, in addition to the Kepler potential, only the J_2 zonal harmonic is taken into consideration, the total specific gravitational potential $V = V(\mathbf{r})$ is given by Vallado (2001):

$$V(\mathbf{r}) = -\frac{\mu}{r}\left\{1 + \frac{\mu J_2 r_{eq}^2}{2r^3}\left[1 - 3\left(\hat{\mathbf{r}}\cdot\mathbf{i}_z\right)^2\right]\right\}, \tag{1}$$

where $\mathbf{r} \in \mathbb{R}^3$ is the position vector in an inertial planetocentric frame, μ denotes the gravitational parameter, J_2 is the second zonal harmonic, r_{eq} is the mean equatorial radius, $\mathbf{i}_z$

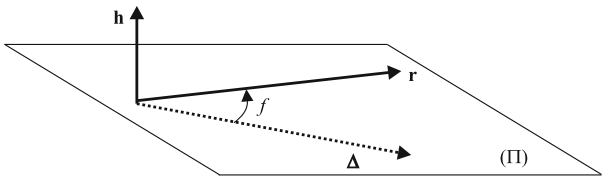

Fig. 1 Definition of the reference axis in the plane of motion

is the unit vector associated with the rotational symmetry axis of the planet, $\hat{\mathbf{r}} = \mathbf{r}/r$, and $r = \|\mathbf{r}\|$.

It is known that the equatorial plane is a relative equilibrium for the aforementioned potential, in the sense that the motion defined by the Initial Value Problem (IVP):

$$\begin{cases} \ddot{\mathbf{r}} = -\dfrac{\partial V}{\partial \mathbf{r}} \\ \begin{cases} \mathbf{r}(t_0) = \mathbf{r}_0; & \mathbf{r}_0 \cdot \mathbf{i}_z = 0 \\ \dot{\mathbf{r}}(t_0) = \mathbf{v}_0; & \mathbf{v}_0 \cdot \mathbf{i}_z = 0 \end{cases} \end{cases} \tag{2}$$

satisfies:

$$\mathbf{r}(t) \cdot \mathbf{i}_z = 0; \ \dot{\mathbf{r}}(t) \cdot \mathbf{i}_z = 0, \ t \geq t_0, \tag{3}$$

where $t_0 \geq 0$ denotes the initial moment of time. Thus, the motion described by IVP (2) is equivalent to the motion which takes place under the influence of the potential field given by:

$$V_{cen}(r) = -\frac{\mu}{r}\left(1 + \frac{J_2 r_{eq}^2}{2r^2}\right), \tag{4}$$

which will be referred to as J_2 *central* potential. The potential defined in Eq. (4) depends only on the distance to the attraction center; therefore, it defines a central force field.

The first integrals of the IVP (2) are the specific total energy

$$\mathcal{E} \triangleq \frac{1}{2}\dot{\mathbf{r}} \cdot \dot{\mathbf{r}} - \frac{\mu}{r} - \frac{\mu J_2 r_{eq}^2}{2r^3} = \frac{1}{2}\mathbf{v}_0 \cdot \mathbf{v}_0 - \frac{\mu}{r_0} - \frac{\mu J_2 r_{eq}^2}{2r_0^3}, \tag{5}$$

and the specific angular momentum vector:

$$\mathbf{h} \triangleq \mathbf{r} \times \dot{\mathbf{r}} = \mathbf{r}_0 \times \mathbf{v}_0. \tag{6}$$

From the initial conditions of the IVP (2), it follows that:

$$\mathbf{h} \times \mathbf{i}_z = \mathbf{0}. \tag{7}$$

The motion modeled by the IVP (2) takes place in the equatorial plane of the planet. Define an oriented fixed reference axis $\mathbf{\Delta}$ in this plane, such that it points to the point on the trajectory which is closest to the attraction center, and denote by f the angle between the position vector $\mathbf{r}$ and the axis $\mathbf{\Delta}$, measured in the sense given by the orientation of vector $\mathbf{h}$ (also see Fig. 1).

Define the effective specific potential energy of the radial motion $U = U(r)$ to be (Arnold et al. 2006):

$$U(r) = \frac{h^2}{2r^2} + V_{cen}(r) = \frac{h^2}{2r^2} - \frac{\mu}{r} - \frac{\mu J}{r^3}, \tag{8}$$

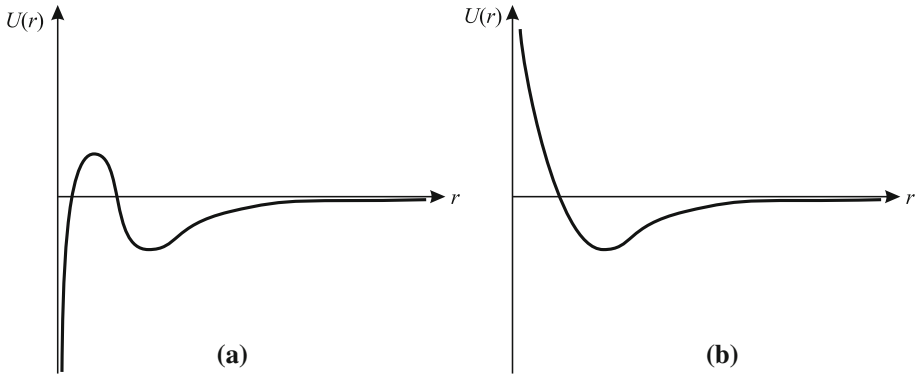

Fig. 2 The effective specific potential energy: **a** J_2 central potential; **b** Newtonian potential

where

$$J = \frac{J_2 r_{eq}^2}{2}. \tag{9}$$

A qualitative description of the function $U(r)$ is depicted in Fig. 2a. For comparison, the effective potential energy associated with the motion in a Newtonian potential (Keplerian motion) is depicted in Fig. 2b.

The effective specific potential energy U is positive if and only if

$$\left(\frac{h^2}{\mu}\right)^2 \geq 16J \tag{10}$$

and the values of the radius vector satisfying the equation $U(r) = 0$ are: $r \in \{r_1, r_2\}$, $0 < r_1 < r_2$, where:

$$r_{1,2} = \frac{1}{4}\left[\frac{h^2}{\mu} \mp \sqrt{\left(\frac{h^2}{\mu}\right)^2 - 16J}\right]. \tag{11}$$

The local extrema of the function $U = U(r)$ are computed as the solutions to the equation

$$\frac{\mathrm{d}U}{\mathrm{d}r} = 0, \tag{12}$$

and are determined to be $0 < r_3 < r_4$:

$$r_{3,4} = \frac{1}{2}\left[\frac{h^2}{\mu} \mp \sqrt{\left(\frac{h^2}{\mu}\right)^2 - 12J}\right]. \tag{13}$$

It may be seen that, similar to the Kepler case, a classification of the motion with respect to the sign of the specific energy $\mathcal{E}$ can be made. If $\mathcal{E} < 0$, then the motion is bounded (depending on the initial conditions), while if $\mathcal{E} \geq 0$, the motion is unbounded.

The polar equations of motion (r, f) are:

$$\begin{cases} \dot{r}^2 = 2\left[\mathcal{E} - U(r)\right]; & r(t_0) = r_0, \\ \dot{f} = \dfrac{h}{r^2}; & f(t_0) = f_0. \end{cases} \tag{14}$$

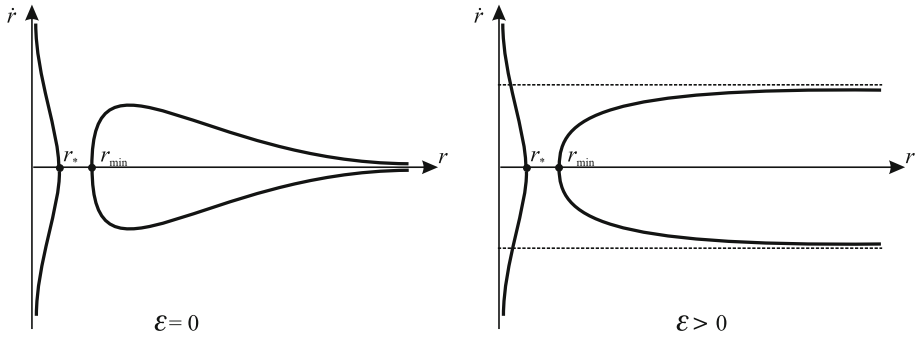

Fig. 3 Examples of phase space curves associated with the radial motion for a given constant positive energy

The orbit in the phase plane $(r, \dot{r})$ associated with a constant energy level $\mathcal{E}$ depends also on the solutions of the algebraic equation:

$$2\left[\mathcal{E} - U\left(r\right)\right] = 0, \tag{15}$$

which is equivalent to:

$$\mathcal{E} - \frac{h^2}{2r^2} + \frac{\mu}{r} + \frac{\mu J}{r^3} = 0. \tag{16}$$

The case $\mathcal{E} < 0$ was studied by Jezewski (1983) and Martinusi and Gurfil (2011). While some of the tools employed hereafter are somewhat similar to the aforementioned works, the present approach will offer a comprehensive insight, together with analytical solutions, for the case $\mathcal{E} \geq 0$. The discussion is structured according to the phase-plane constant energy curves depicted qualitatively in Fig. 3, and the two cases are: (i) zero specific energy $\mathcal{E} = 0$, which implies $\dot{r} \to 0$ as $r \to \infty$ and (ii) strictly positive specific energy $\mathcal{E} > 0$, which implies $\dot{r} \to \text{const.} > 0$ as $r \to \infty$.

Under certain specific initial conditions, the orbits in the phase plane $(r, \dot{r})$ intersect the r axis in two points, located on two separate branches (see Fig. 3). These points are associated with the roots of the algebraic equation (15). The branch intersecting the r-axis at $r = r_*$ is associated with the collision with the attraction center as $r \to 0$, and has no apparent physical meaning (usually, $r_* < r_{eq}$, where r_{eq} is the mean equatorial radius, so the orbit would be below the planet's surface). Because of this reason, the other positive root of Eq. (16) is denoted by $r_{\min}$, as it constitutes the point on the trajectory which is closest to the attraction center.

The reference axis $\mathbf{\Delta}$ is chosen so it passes through the attraction center and the closest point on the trajectory, which is named the *pericenter* of the orbit. The angle f is initialized as 0 when the position vector has the same orientation as $\mathbf{\Delta}$, and is referred to as the *polar angle*.

3 Pseudo-parabolic orbits

When the total specific energy $\mathcal{E} = 0$, the equations of motion (14) transform into:

$$\begin{cases} \dot{r}^2 = \dfrac{2\mu\left(r - r_*\right)\left(r - r_{\min}\right)}{r^3}; & r\left(t_0\right) = r_0, \\ \dot{f} = \dfrac{h}{r^2}; & f\left(t_0\right) = f_0. \end{cases} \tag{17}$$

The solutions $0 < r_* < r_{\min}$ for the equation $\dot{r} = 0$ are determined as:

$$r_*, r_{\min} = \frac{1}{2}\left(\frac{h^2}{2\mu} \mp \sqrt{\frac{h^4}{4\mu^2} - 4J}\right); \tag{18}$$

The expression for the polar angle $f = f(r)$ may be derived from:

$$f(r) = \pm \int_{r_{\min}}^{r} \frac{hs^{-\frac{1}{2}}}{\sqrt{2\mu(s - r_*)(s - r_{\min})}} \mathrm{d}s, \tag{19}$$

where the sign "+" is chosen when $\mathbf{r} \cdot \dot{\mathbf{r}} \geq 0$ and "−" otherwise. The integral in Eq. (19) yields:

$$f(r) = \pm \frac{2h}{\sqrt{2\mu r_{\min}}} F\left(\sqrt{\frac{r - r_{\min}}{r - r_*}}, \sqrt{\frac{r_*}{r_{\min}}}\right), \tag{20}$$

where $F(\cdot, \cdot)$ denotes the incomplete elliptic integral of the first kind, written in the Jacobi form, defined by:

$$F(z, k) \triangleq \int_0^z \frac{\mathrm{d}u}{\sqrt{1 - u^2}\sqrt{1 - k^2 u^2}}. \tag{21}$$

Make the additional notations:

$$h_* = \sqrt{2\mu r_{\min}}, \quad p_* = 2r_{\min}, \quad w = \sqrt{\frac{r_*}{r_{\min}}}, \quad \lambda(r) = \sqrt{\frac{r - r_{\min}}{r - r_*}}, \tag{22}$$

and define:

$$\beta \triangleq \sqrt{1 + \frac{r_*}{r_{\min}}} = \sqrt{1 + w^2} = \sqrt{1 + \frac{2r_*}{p_*}} = \frac{h_*}{h}. \tag{23}$$

Then Eq. (20) may be written in the compact form:

$$f(r) = \pm 2\beta F(\lambda(r), w). \tag{24}$$

The value of the polar angle f as the magnitude $r \to \infty$ defines the angle between the symmetry axis of the orbit and one of the asymptotic directions, and is defined by:

$$f_{\max} = 2\beta F(1, w). \tag{25}$$

The polar equation of the trajectory in the form $r = r(f)$ may be deduced from Eq. (24) as:

$$r(f) = \frac{r_{\min}}{\mathrm{sn}^2(\chi(f), w)}, \tag{26}$$

where $\chi = \chi(f)$ is defined by:

$$\chi(f) = \frac{f_{\max} - f}{2\beta}. \tag{27}$$

and "sn" denotes the Jacobi elliptic sine (Abramowitz and Stegun 1964).

From the first of Eq. (17), the implicit expression of the magnitude $r = r(t)$ with respect to the time variable may be derived as:

$$t(r) = t_0 \pm \int_{r_0}^{r} \frac{s^{3/2}}{\sqrt{2\mu(s - r_*)(s - r_{\min})}} \mathrm{d}s, \tag{28}$$

where the sign "+" is chosen if $\mathbf{r} \cdot \dot{\mathbf{r}} \geq 0$ and "−" otherwise. After some computations, Eq. (28) yields:

$$t(r) = t_0 \pm [\eta(r) - \eta(r_0)], \tag{29}$$

where $\eta = \eta(r)$ is defined as:

$$\eta(r) = \int_{r_{\min}}^{r} \frac{s^{3/2}}{\sqrt{2\mu(s - r_*)(s - r_{\min})}} \mathrm{d}s, \tag{30}$$

yielding the expression:

$$\begin{aligned} \eta(r) = \frac{2}{3\sqrt{2\mu}} \Big\{ & \sqrt{r}\lambda(r)(r + r_* + 2r_{\min}) \\ & + \sqrt{r_{\min}}\left[(2r_{\min} + r_*) F(\lambda(r), w) - 2(r_{\min} + r_*) E(\lambda(r), w)\right] \Big\}, \end{aligned} \tag{31}$$

where $E(\cdot, \cdot)$ denotes the incomplete elliptic integral of the second kind, defined in the Jacobi form as:

$$E(z, k) = \int_0^z \frac{\sqrt{1 - k^2 u^2}\mathrm{d}u}{\sqrt{1 - u^2}} \tag{32}$$

Let t_P be the time of periapsis passage. Then its value may be computed from the initial conditions by taking into account Eq. (29), as well as:

$$t_P = t(r_{\min}). \tag{33}$$

The following expression holds:

$$t_P = t_0 \mp \eta(r_0). \tag{34}$$

The interpretation of the above choice of signs is the following: If $\mathbf{r}_0 \cdot \mathbf{v}_0 \geq 0$, then the magnitude of the position vector is instantaneously increasing at the initial moment of time, which means that the time of pericenter passage is before t_0, and therefore $t_P \leq t_0$. If $\mathbf{r}_0 \cdot \mathbf{v}_0 < 0$, then the magnitude of the position vector is decreasing towards $r_{\min}$, so the spacecraft will pass through the pericenter after the initial moment of time, yielding $t_0 < t_P$.

3.1 The "fish" orbit

Equation (26) gives the polar equation of the trajectory in the plane of motion, which is orthogonal to the specific angular momentum vector $\mathbf{h}$ (defined in Eq. (6)) and passes through the attraction center. From Eq. (26) it follows that the trajectory is a curve which has $\mathbf{\Delta}$ as a symmetry axis.

An interesting feature of the trajectory is that it self-intersects at a point situated on the symmetry axis (unlike the parabolic Keplerian counterpart). This is due to the fact that $f > \pi$ as $r \to \infty$, which is seen from:

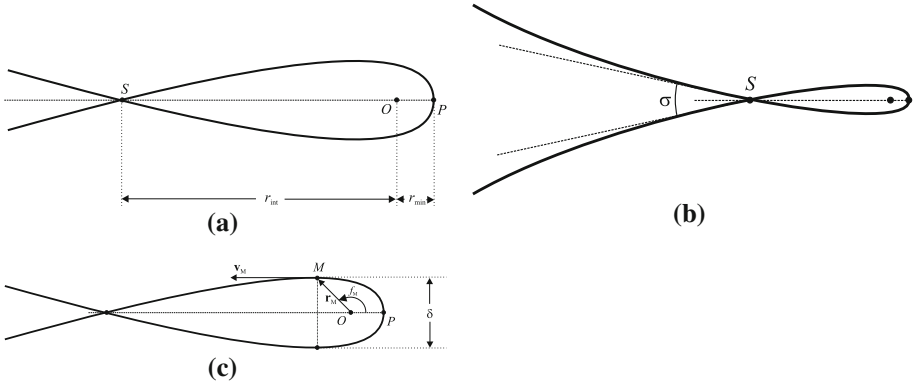

Fig. 4 The pseudo-parabolic trajectory (the "fish" orbit) in a J_2 central field. **a** A general description. **b** The angle between the tangents at point S. **c** The aperture of the closed loop

$$f_{\max} = f(\infty) = 2\beta \lim_{r\to\infty} E(\lambda(r), w), \tag{35}$$

yielding:

$$f_{\max} \stackrel{\Delta}{=} 2\beta E(1, w). \tag{36}$$

The trajectory is described qualitatively in Fig. 4a. The distance between the self-intersection point of the trajectory and the attraction center may be determined by solving:

$$f(r) = \pi, \tag{37}$$

which yields:

$$r_{int} = r(\pi) = \frac{r_{\min}}{\operatorname{sn}^2\left(\dfrac{f_{\max} - \pi}{2\beta}, w\right)} \tag{38}$$

The vector expressions for the position and velocity associated with the pseudo-parabolic motion may be written with respect to a perifocal reference frame $\{\mathbf{i}_1, \mathbf{i}_2, \mathbf{i}_3\}$, where $\mathbf{i}_1$ is the unit vector associated with the reference axis $\boldsymbol{\Delta}$, $\mathbf{i}_3$ is the unit vector of the specific angular momentum, and $\mathbf{i}_2$ completes a right handed orthogonal frame.

Then the state of the spacecraft with respect to this reference frame may be expressed as:

$$\begin{cases} \mathbf{r} = r\left[(\cos f)\,\mathbf{i}_1 + (\sin f)\,\mathbf{i}_2\right], \\ \dot{\mathbf{r}} = \left(\dot{r}\cos f - \dfrac{h}{r}\sin f\right)\mathbf{i}_1 + \left(\dot{r}\sin f + \dfrac{h}{r}\cos f\right)\mathbf{i}_2, \end{cases} \tag{39}$$

where r is expressed in Eq. (26), while $\dot{r}$ is determined from the first of Eq. (17):

$$\dot{r} = \pm\frac{\sqrt{2\mu(r - r_*)(r - r_{\min})}}{r^{3/2}}. \tag{40}$$

The sign "+" is chosen if $f \in [0, f_{\max})$ and "−" otherwise.

The expression for the initial polar angle $f_0 = f(t_0)$ may be computed from Eq. (20) by substituting $r = r_0$. It follows that:

$$f_0 = \pm 2\beta F(\lambda(r_0), w), \tag{41}$$

where the sign "+" is chosen if $\mathbf{r}_0 \cdot \mathbf{v}_0 \geq 0$ and "−" otherwise. The unit vector $\mathbf{i}_1$ may be determined from the initial conditions as follows:

$$\mathbf{i}_1 = (\cos f_0)\,\hat{\mathbf{r}}_0 - (\sin f_0)\,\hat{\mathbf{h}} \times \hat{\mathbf{r}}_0, \tag{42}$$

while the unit vector $\mathbf{i}_2$ is determined as:

$$\mathbf{i}_2 = (\sin f_0)\,\hat{\mathbf{r}}_0 + (\cos f_0)\,\hat{\mathbf{h}} \times \hat{\mathbf{r}}_0. \tag{43}$$

Four more quantities remain to be determined for the trajectory depicted in Fig. 4a: The angle between the tangents at the orbit in the point S, the aperture of the closed loop of the trajectory, the time spent inside the closed loop and the behavior at infinity of the trajectory.

Denote by σ the angle between the tangents of the trajectory at point S (see Fig. 4b). Then

$$\cos\frac{\sigma}{2} = -\frac{\dot{\mathbf{r}}(\pi)}{\|\dot{\mathbf{r}}(\pi)\|} \cdot \mathbf{i}_1. \tag{44}$$

The expression for $\dot{\mathbf{r}}(\pi) \cdot \mathbf{i}_1$ is obtained from the second of Eq. (39):

$$\dot{\mathbf{r}}(\pi) \cdot \mathbf{i}_1 = -\frac{\sqrt{2\mu\,[r(\pi) - r_*]\,[r(\pi) - r_{\min}]}}{r^{3/2}} \tag{45}$$

while the magnitude of the velocity $\|\dot{\mathbf{r}}(\pi)\|$ may be recovered from the conservation of the total specific energy:

$$\|\dot{\mathbf{r}}(\pi)\| = \sqrt{\frac{2\mu}{r(\pi)} + \frac{2\mu J}{r^3(\pi)}}. \tag{46}$$

It follows that the value of angle $\sigma \in [0, \pi]$ is computed from:

$$\sigma = 2\cos^{-1}\sqrt{\frac{[r(\pi) - r_*]\,[r(\pi) - r_{\min}]}{r^2(\pi) + J}}, \tag{47}$$

where $r(\pi) = r_{int}$ is expressed in Eq. (38).

The aperture of the closed loop of the orbit is determined by considering the following rationale (cf. Fig. 4c): On the closed loop, the spacecraft is at the maximum distance from the symmetry axis at a given point M, which occurs at the moment when the velocity has the same direction as the symmetry axis $\boldsymbol{\Delta}$, which yields:

$$\begin{cases} \dot{r}_M \sin f_M + \dfrac{h}{r_M}\cos f_M = 0 \\ \\ \dot{r}_M \cos f_M - \dfrac{h}{r_M}\sin f_M = -\sqrt{\dfrac{2\mu}{r_M} + \dfrac{2\mu J}{r_M^3}} \end{cases} \tag{48}$$

In Eq. (48), one has to take into account:

$$\dot{r}_M = \frac{\sqrt{2\mu\,(r_M - r_*)\,(r_M - r_{\min})}}{r_M^{3/2}}, \tag{49}$$

and also:

$$\dot{r}_M^2 + \frac{h^2}{r_M^2} = 2\left(\frac{\mu}{r_M} + \frac{\mu J}{r_M^3}\right). \tag{50}$$

By making some simple trigonometric manipulations on Eq. (48), it follows that:

$$f_M = \pi - \phi, \tag{51}$$

where ϕ is defined by:

$$\begin{cases} \sin\phi = \dfrac{h}{\sqrt{2\mu}}\sqrt{\dfrac{r_M}{r_M^2 + J}} \\ \\ \cos\phi = \sqrt{\dfrac{[r_M - r_*]\,[r_M - r_{\min}]}{r_M^2 + J}} \end{cases} \tag{52}$$

It follows that the aperture δ of the closed loop is:

$$\delta = 2\frac{hr_M}{\sqrt{2\mu}}\sqrt{\frac{r_M}{r_M^2 + J}}. \tag{53}$$

The value of r_M is determined by noticing that from Eq. (51),

$$\sin f_M = \sin\phi, \tag{54}$$

which yields [also by taking into account Eq. (20)]:

$$\sin\left[2\beta F\left(\lambda\left(r_M\right), w\right)\right] = \frac{h}{\sqrt{2\mu}}\sqrt{\frac{r_M}{r_M^2 + J}}. \tag{55}$$

After numerically solving the transcendental equation (55), the expression of the aperture in Eq. (53) may be computed.

The length of the time interval necessary for the spacecraft to complete the entire closed loop of the trajectory (from point S through the pericenter and then back to point S) may be computed easily due to the symmetry of the trajectory, and its expression is:

$$T_{loop} = 2\int_{r_{\min}}^{r_{int}} \frac{s^{3/2}}{\sqrt{2\mu\,(s - r_*)\,(s - r_{\min})}}\mathrm{d}s, \tag{56}$$

which leads to the expression:

$$T_{loop} = 2\eta\left(r_{int}\right), \tag{57}$$

where $\eta = \eta(r)$ is defined in Eq. (31).

In order to determine the behavior at infinity on one of the unbounded arcs, consider a generic point Q on the trajectory, outside the closed loop, and denote by $\mathbf{r}_Q$ its position vector with respect to an inertial reference frame $X'OY'$, which is rotated with respect to $\{\mathbf{i}_1, \mathbf{i}_2\}$ with the angle $f_{\max} - \pi$ in the sense given by the angular momentum vector (cf. Fig. 5). Then the Cartesian projections of r_Q on the axis of this frame are expressed as:

$$\begin{cases} r_1 = r_Q\cos\left(\pi + f - f_{\max}\right) = -r_Q\cos\left(f_{\max} - f\right) \\ \\ r_2 = r_Q\sin\left(\pi + f - f_{\max}\right) = r_Q\sin\left(f_{\max} - f\right) \end{cases} \tag{58}$$

It may be seen that $r_{1,2} \to \infty$ as $r \to \infty$, but the ratio

$$m(f) = \frac{r_2}{r_1} = \tan\left(f_{\max} - f\right) \tag{59}$$

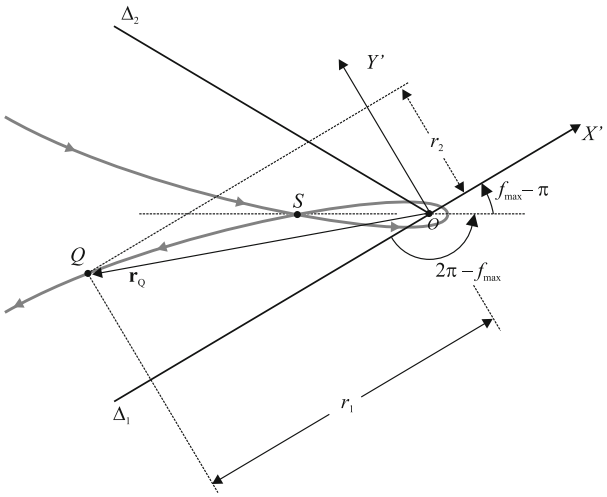

Fig. 5 The behavior of the pseudo-parabola at infinity

satisfies $m\left(f_{\max}\right)=0$. It follows that there exist no asymptotes for the unbounded arcs of the pseudo-parabola. Instead, there exists an asymptotic direction of the trajectory, which forms the angle $f_{\max}-\pi$ with the symmetry axis.

4 Pseudo-hyperbolic orbits

If $\mathcal{E}>0$, the solutions for $\dot{r}=0$ are obtained by solving the cubic algebraic equation

$$r^3+\frac{\mu}{\mathcal{E}}r^2-\frac{h^2}{2\mathcal{E}}r+\frac{\mu J}{\mathcal{E}}=0, \tag{60}$$

which leads to the roots $r_{neg}<0<r_*<r_{\min}$. Denote:

$$r_M=-r_{neg}>0. \tag{61}$$

From the Vieta formulae associated to Eq. (60) it is deduced that:

$$r_*=J\frac{r_M-r_{\min}}{r_{\min}r_M+J}. \tag{62}$$

The polar equations of motion may now be rewritten as:

$$\begin{cases}\dot{r}^2=\dfrac{2\mathcal{E}\left(r+r_M\right)\left(r-r_*\right)\left(r-r_{\min}\right)}{r^3}; & r\left(t_0\right)=r_0;\\ \dot{f}=\dfrac{h}{r^2}; & f\left(t_0\right)=f_0.\end{cases} \tag{63}$$

The expression for $f=f\left(r\right)$ is

$$f\left(r\right)=\pm\int_{r_{\min}}^{r}\frac{hs^{-1/2}\mathrm{d}s}{\sqrt{2\mathcal{E}\left(s+r_M\right)\left(s-r_*\right)\left(s-r_{\min}\right)}} \tag{64}$$

where the sign "+" is used if $\mathbf{r}\cdot\dot{\mathbf{r}}\geq 0$ and the sign "−" otherwise. The integral in Eq. (64) has the expression:

$$f(r)=\pm\frac{2h}{\sqrt{2\mathcal{E}r_{\min}(r_M+r_*)}}F\left(\sqrt{\frac{(r_M+r_*)(r-r_{\min})}{(r_M+r_{\min})(r-r_*)}},w\right), \tag{65}$$

where w is defined as:

$$w=\sqrt{\frac{r_*(r_{\min}+r_M)}{r_{\min}(r_*+r_M)}}. \tag{66}$$

Make the additional notations:

$$a_*\triangleq\frac{r_M-r_{\min}}{2};\quad e_*\triangleq\frac{r_M+r_{\min}}{r_M-r_{\min}}>1;\quad p_*\triangleq a_*\left(e_*^2-1\right), \tag{67}$$

and

$$\begin{cases}\alpha\triangleq\sqrt{\dfrac{\mu}{(r_M-r_{\min})\mathcal{E}}}=\sqrt{1-\dfrac{r_*}{2a_*}};\\[2ex]\beta\triangleq\dfrac{h}{\sqrt{2\mathcal{E}r_Mr_{\min}}}=\sqrt{1-\dfrac{2r_*}{p_*}};\\[2ex]\gamma\triangleq\dfrac{h}{\sqrt{2\mathcal{E}r_{\min}(r_M+r_*)}}=\beta\sqrt{1-\dfrac{r_*}{r_M+r_*}}.\end{cases} \tag{68}$$

Then the expression for the polar angle f from Eq. (65) becomes:

$$f(r)=\pm 2\gamma F\left(\sqrt{\frac{(r_M+r_*)(r-r_{\min})}{(r_M+r_{\min})(r-r_*)}},w\right), \tag{69}$$

In Eq. (69), the sign "+" is chosen if $\mathbf{r}\cdot\dot{\mathbf{r}}\geq 0$ and "−" otherwise.

From Eq. (63), the implicit expression of the magnitude $r=r(t)$ with respect to the time variable may be derived as:

$$t(r)=t_0\pm\int_{r_0}^{r}\frac{s^{3/2}}{\sqrt{2\mathcal{E}(s+r_M)(s-r_*)(s-r_{\min})}}\mathrm{d}s, \tag{70}$$

where the sign "+" is chosen if $\mathbf{r}\cdot\dot{\mathbf{r}}\geq 0$ and "−" otherwise. Denote:

$$\sigma_1(r)=\int_{r_{\min}}^{r}\frac{s^{3/2}}{\sqrt{2\mathcal{E}(s+r_M)(s-r_*)(s-r_{\min})}}\mathrm{d}s. \tag{71}$$

Then the integral in Eq. (70) is computed as:

$$t(r)=t_0\pm\left[\sigma_1(r)-\sigma_1(r_0)\right]. \tag{72}$$

The expression for the integral $\sigma_1(r)$ is computed as:

$$\begin{aligned}\sigma_1(r)=&\frac{1}{\sqrt{2\mathcal{E}}}\left[C_1F(\xi(r),w)-C_2E(\xi(r),w)-C_3\Pi\left(\xi(r),\frac{r_M+r_{\min}}{r_M+r_*},w\right)\right]\\&+\frac{1}{\sqrt{2\mathcal{E}}}\frac{r^2}{(r-r_*)}\sqrt{1-\frac{U(r)}{2\mathcal{E}}},\end{aligned} \tag{73}$$

where the following notations were used:

$$\begin{cases} C_1 = C_2 - \dfrac{r_* \left(r_M - r_*\right)}{C_2}; \quad C_3 = \dfrac{\mu \left(r_{\min} - r_*\right)}{\mathcal{E} C_2}; \\ C_2 = \sqrt{r_{\min} \left(r_M + r_*\right)}; \qquad \xi \left(r\right) = \sqrt{\dfrac{r_M + r_*}{r_M + r_{\min}}} \sqrt{\dfrac{r - r_{\min}}{r - r_*}}, \end{cases} \tag{74}$$

$\Pi \left(\cdot, \cdot, \cdot\right)$ denotes the incomplete elliptic integral of the third kind, defined as:

$$\Pi \left(z, \upsilon, k\right) = \int_0^z \frac{\mathrm{d}s}{\sqrt{1 - \upsilon^2 s^2} \sqrt{1 - s^2} \sqrt{1 - k^2 s^2}}$$

and w is defined in Eq. (66).

The moment of time associated with the periapsis passage is computed by substituting $r = r_{\min}$ into Eq. (72), thus obtaining

$$t_P = t_0 \mp \sigma_1 \left(r_0\right), \tag{75}$$

where the sign "−" is chosen if $\mathbf{r} \cdot \dot{\mathbf{r}} \geq 0$ and "+" otherwise.

The interpretation of the choice of the sign in Eqs. (72) and (75) is the same as the one given for the pseudo-parabolic orbit, in Sect. 3.

4.1 Geometry of the orbit

The polar equation of motion (r, f) may be obtained in explicit form $r = r \left(f\right)$ by inverting Eq. (65) and after performing some mathematical manipulations. The magnitude of the position vector is expressed with respect to f as:

$$r \left(f\right) = \frac{r_M r_{\min}}{-r_{\min} + \left(r_M + r_{\min}\right) \mathrm{sn}^2 \left(\chi \left(f\right)\right)}, \tag{76}$$

where:

$$\chi \left(f\right) = F \left(1, w\right) - \frac{f}{2\gamma}. \tag{77}$$

By making use of the notations defined in Eq. (40), expression (76) may be rewritten into:

$$r \left(f\right) = \frac{p_*}{1 + e_* \mathrm{sn}^2 \chi \left(f\right)}. \tag{78}$$

The trajectory has as symmetry axis the line $\mathbf{\Delta}$, which passes through the attraction center and the pericenter of the trajectory, since:

$$r \left(f\right) = r \left(-f\right). \tag{79}$$

Also, the trajectory has two asymptotes for $r \to \infty$. The angle between one asymptote and the symmetry axis is computed based on Eq. (69) as:

$$f_{\max} = f \left(\infty\right) = 2\gamma \lim_{r \to \infty} F \left(\sqrt{\frac{\left(r_M + r_*\right) \left(r - r_{\min}\right)}{\left(r_M + r_{\min}\right) \left(r - r_*\right)}}, w \right) = 2\gamma F \left(\sqrt{\frac{r_M + r_*}{r_M + r_{\min}}}, w \right). \tag{80}$$

The pseudo-hyperbolic trajectory is depicted in Fig. 6.

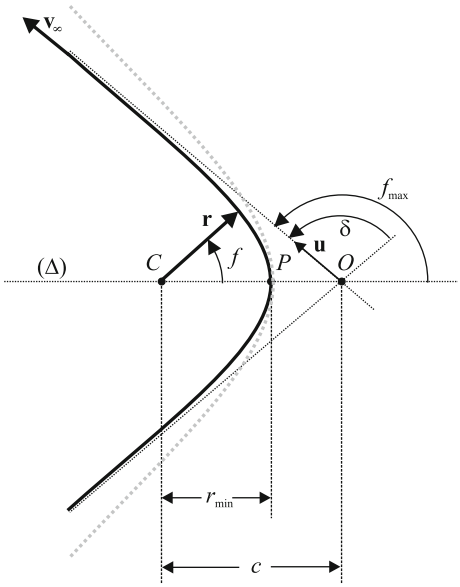

Fig. 6 The pseudo-hyperbolic trajectory. The *dotted* trajectory represents its Keplerian counterpart, sharing the same pericenter $r_{\min}$

The deflection angle is defined to be the angle between the asymptotes. Following the aforementioned considerations, the deflection angle is

$$\delta = 2f_{\max} - \pi = 4\gamma F\left(\sqrt{\frac{r_M + r_*}{r_M + r_{\min}}}, w\right) - \pi. \tag{81}$$

Define the reference frame $\{\mathbf{i}_1, \mathbf{i}_2, \mathbf{i}_3\}$ similarly to the pseudo-parabolic trajectory. The position and velocity vectors associated with the pseudo-hyperbolic motion are identical to the ones in Eq. (39), with the radius r determined in Eqs. (76) or (78). The velocity at infinity is expressed as (cf. Fig. 6):

$$\mathbf{v}_\infty = \sqrt{2\mathcal{E}}\,(-\cos f_{\max}\mathbf{i}_1 + \sin f_{\max}\mathbf{i}_2) = \sqrt{2\mathcal{E}}\mathbf{u}. \tag{82}$$

An interesting relation between the quantities defined for the pseudo-hyperbolic orbit (also useful in the numerical examples and comparisons) is that the pseudo-eccentricity e_* is linked to v_∞ and $r_{\min}$ through

$$e_* = 1 + \frac{r_{\min}^2 v_\infty}{\mu}\alpha^2 \tag{83}$$

The distance c from the attraction center C to the intersection of the asymptotes O is computed as follows: Let d_h be the distance from the attraction center to one of the asymptotes. Then

$$d_h = \frac{h}{v_\infty} = \frac{h}{\sqrt{2\mathcal{E}}} = \beta a_*\sqrt{e_*^2 - 1}. \tag{84}$$

The distance c_h is determined as:

$$c_h = \frac{d_h}{\tan f_{\max}} = \frac{h}{\sqrt{2\mathcal{E}}\tan f_{\max}}. \tag{85}$$

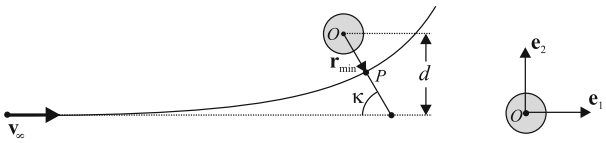

Fig. 7 Approach from infinity in a J_2 central field

4.2 The approach from infinity in a J_2 central field

An important application of the pseudo-hyperbolic motion in a J_2 central force field is the approach from infinity, which offers new insights on the flybys about an oblate spheroidal planet. Some examples show that for a given velocity at infinity, and a given distance from the attraction center to the asymptote, the results could be significantly different than the case of a Keplerian flyby. This difference is quantified by means of expressions for the differences in the deflection angles and the pericenter vectors.

Consider a particle arriving from infinity with the velocity $\mathbf{v}_\infty$, $v_\infty > 0$, and let the distance from the attraction center to the asymptote be denoted by d_h (cf. Fig. 7). It is known that the particle moves on a pseudo-hyperbolic trajectory, in a plane defined by the attraction center and $\mathbf{v}_\infty$. Define an inertial reference frame $\mathcal{R}_O = \{\mathbf{e}_1, \mathbf{e}_2, \mathbf{e}_3\}$ originating from the attraction center, which has the unit vectors defined as:

$$\mathbf{e}_1 = \hat{\mathbf{v}}_\infty; \mathbf{e}_2 = \mathbf{h} \times \mathbf{v}_\infty; \ \mathbf{e}_3 = \hat{\mathbf{h}}. \tag{86}$$

Denote by $\mathbf{r}_{\min}$ the position vector of the pericenter P with respect to the inertial frame $\mathcal{R}_O$.

Since $r_\infty = \infty$, the specific total energy of the pseudo-hyperbolic motion is computed as:

$$\mathcal{E} = \frac{1}{2} v_\infty^2. \tag{87}$$

The magnitude of the angular momentum vector is also computed at this time from:

$$h = v_\infty d_h = \sqrt{2\mathcal{E}} d_h. \tag{88}$$

The distance $r_{\min}$ from the attraction center O to the pericenter P is the positive root of the polynomial equation (60). Let r_* be the other positive root and let $-r_M$ be the negative one. Then the deflection angle is computed by using Eq. (81), while the angle between the pericenter line and the asymptote is expressed as:

$$\kappa = \pi - f_{\max} = \pi - 2\gamma F\left(\sqrt{\frac{r_M + r_*}{r_M + r_{\min}}}, w\right). \tag{89}$$

With respect to the reference frame $\mathcal{R}_O$, the vector $\mathbf{r}_{\min}$ can be written as:

$$\mathbf{r}_{\min} = r_{\min}\left(\cos\kappa \mathbf{e}_1 - \sin\kappa \mathbf{e}_2\right) = -r_{\min}\left(\cos f_{\max} \mathbf{e}_1 + \sin f_{\max} \mathbf{e}_2\right). \tag{90}$$

4.2.1 Comparison with the Keplerian model

Two scenarios are compared: (i) arrival from infinity in a J_2 central field and (ii) arrival from infinity assuming a Keplerian model. The initial conditions are set to be in the same plane. They are chosen independently of the gravitational model.

The point of the injection, the magnitude of the velocity at infinity v_∞, as well as the distance d_h, are given as initial conditions. The specific total energy and the specific angular momentum magnitude are determined as:

$$\mathcal{E} = \frac{v_\infty^2}{2}, \quad h = d_h v_\infty. \tag{91}$$

Assume first that a Keplerian gravitational model is considered. The semimajor axis is:

$$a = \frac{\mu}{2\mathcal{E}} = \frac{\mu}{v_\infty^2}, \tag{92}$$

and the eccentricity is determined as:

$$e = \sqrt{1 + \frac{d_h^2 v_\infty^4}{\mu^2}}. \tag{93}$$

The minimum distance to the attraction center is computed as:

$$r_{\min} = a\,(e-1) = \frac{d_h \mu}{\sqrt{d_h^2 v_\infty^4 + \mu^2} + \mu}. \tag{94}$$

By following the Keplerian approach, the deflection angle is computed as:

$$\delta_{Kep} = \pi - 2\cos^{-1}\left(\frac{1}{e}\right) = \pi - 2\cos^{-1}\frac{\mu}{\sqrt{d^2 v_\infty^4 + \mu^2}}, \tag{95}$$

which yields:

$$\sin\delta_{Kep} = \frac{2\mu d v_\infty^2}{d^2 v_\infty^4 + \mu^2}; \quad \cos\delta_{Kep} = \frac{d^2 v_\infty^4 - \mu^2}{d^2 v_\infty^4 + \mu^2}. \tag{96}$$

The vector $\mathbf{r}_{\min}^{Kep}$ is determined to be:

$$\mathbf{r}_{\min}^{Kep} = -r_{\min}\left(\cos\delta_{Kep}\mathbf{e}_1 + \sin\delta_{Kep}\mathbf{e}_2\right), \tag{97}$$

which yields:

$$\mathbf{r}_{\min}^{Kep} = -\frac{d\mu}{\sqrt{d^2 v_\infty^4 + \mu^2} + \mu}\left(\frac{d^2 v_\infty^4 - \mu^2}{d^2 v_\infty^4 + \mu^2}\mathbf{e}_1 + \frac{2\mu d v_\infty^2}{d^2 v_\infty^4 + \mu^2}\mathbf{e}_2\right). \tag{98}$$

Assume now that a J_2 central gravitational model is considered. The expressions for the total specific energy, as well as for the angular momentum, remain as expressed in Eq. (91), while the minimum distance to the attraction center $r_{\min}$ is determined by solving the polynomial equation (60). The deflection angle is computed by using Eq. (81), while the position of the pericenter in the inertial frame $\{\mathbf{i}_1, \mathbf{i}_2\}$ is the one expressed in Eq. (90). The following differences may now be computed:

The difference in deflection angles:

$$\Delta\delta_{def} = \delta - \delta_{Kep} = 2\arccos\frac{\mu}{\sqrt{d^2 v_\infty^4 + \mu^2}} - 4\gamma F\left(\sqrt{\frac{r_M + r_*}{r_M + r_{\min}}}, \sqrt{\frac{r_* (r_{\min} + r_M)}{r_{\min}(r_* + r_M)}}\right). \tag{99}$$

The difference in pericenter distances:

$$\Delta r_{\min} = r_{\min} - r_{\min}^{Kep} = r_{\min} - \frac{d\mu}{\sqrt{d^2 v_\infty^4 + \mu^2} + \mu}. \tag{100}$$

The difference in the position vector of the pericenter:

$$\begin{aligned}\mathbf{r}_{\min} - \mathbf{r}_{\min}^{Kep} = & \frac{\mu d}{\sqrt{d^2 v_\infty^4 + \mu^2} + \mu} \left(\frac{d^2 v_\infty^4 - \mu^2}{d^2 v_\infty^4 + \mu^2} \mathbf{e}_1 + \frac{2\mu d v_\infty^2}{d^2 v_\infty^4 + \mu^2} \mathbf{e}_2 \right) \\ & - r_{\min} \left(\cos f_{\max} \mathbf{e}_1 + \sin f_{\max} \mathbf{e}_2 \right).\end{aligned} \tag{101}$$

Some illustrative examples related to the above derivations are presented in Sect. 5.

4.3 The eccentricity vector

The solutions presented above for the pseudo-parabolic and pseudo-hyperbolic orbits were expressed with respect to the frame $\{\mathbf{i}_1, \mathbf{i}_2, \mathbf{i}_3\}$, defined in Sect. 2.

A natural problem arising from these considerations is to derive the expression for the vector $\mathbf{i}_1$ from the state of the spacecraft (position and velocity) at any moment of time, thus defining the vectorial orbital elements of the orbit. The expression for $\mathbf{i}_1$ may be recovered at any moment of time by using the expression (Battin 1999):

$$\mathbf{i}_1 = (\cos f)\, \mathbf{i}_r - (\sin f)\, \mathbf{i}_\theta, \tag{102}$$

where:

$$\mathbf{i}_r = \hat{\mathbf{r}}, \quad \mathbf{i}_\theta = \hat{\mathbf{h}} \times \hat{\mathbf{r}}. \tag{103}$$

An expression for $f(r)$ may be recovered from Eq. (20) for the pseudo-parabolic orbit and from Eq. (69) for the pseudo-hyperbolic orbit. The following expressions are obtained:

Pseudo-parabolic orbit:

$$f(\mathbf{r}, \dot{\mathbf{r}}) = 2\sqrt{1 + \frac{r_*}{r_{\min}}}\, F\left(\sqrt{\frac{r}{2\mu}} \mathbf{r} \cdot \dot{\mathbf{r}}, \sqrt{\frac{r_*}{r_{\min}}} \right) \tag{104}$$

Pseudo-hyperbolic orbit:

$$f(\mathbf{r}, \dot{\mathbf{r}}) = \frac{2\beta}{\sqrt{p_* + r_* (e_* - 1)}} F\left(\frac{\beta}{\rho h} \sqrt{\frac{r}{r - r_*} \frac{p_* r_*}{p_* + r (e_* - 1)}} (\mathbf{r} \cdot \dot{\mathbf{r}}), \rho \right), \tag{105}$$

where

$$\rho = \sqrt{\frac{2 r_* e_*}{p_* + r_* (e_* - 1)}}. \tag{106}$$

By substituting Eqs. (104) and (105) into Eq. (102), the expression for $\mathbf{i}_1$ is obtained for the pseudo-parabolic and pseudo-hyperbolic cases, respectively, in the classical form of a vectorial first integral:

$$\mathbf{i}_1 = \mathbf{i}_1 (\mathbf{r}, \dot{\mathbf{r}}, \mathbf{r}_0, \mathbf{v}_0). \tag{107}$$

The vectorial orbital elements defining the trajectory (in both cases) are $\mathbf{h}$ and $\mathbf{i}_1$. The position on the trajectory is determined based on f, and may also be propagated with respect to time by making use of the vectorial solution in each case.

5 Numerical examples

5.1 Pseudo-parabolic ("fish") orbits

Three examples are presented. The difference in escape velocities is investigated and the pseudo-parabolic motion is compared to a Keplerian motion, for an injection from the (common) pericenter.

5.1.1 Differences in the escape velocities

Tables 1, 2 and 3 present the escape velocities $|\mathbf{v}_{esc}|$ computed based on the Keplerian model and the J_2 central model, for Earth, Venus and Jupiter, for altitudes above the surface of the planet varying from 0 up to 40, 000 km. The J_2 central escape velocity is slightly larger than its Keplerian counterpart:

$$v_{esc}^{Kep} = \sqrt{\frac{2\mu}{r}}; \quad v_{esc}^{J_2} = \sqrt{\frac{2\mu}{r} + \frac{\mu J_2 r_{eq}^2}{r^3}}. \tag{108}$$

As expected, the effect of J_2 is of order 10^{-3} at the surface of the planet, and decreases with the altitude.

Table 1 Comparison of escape velocities (Keplerian versus J_2 central), Earth; $r_{eq} = 6378.16 \cdot 10^3$ m; $\mu = 3.986012 \cdot 10^{14}$ m^3/s^2; $J_2 = 1.082 \cdot 10^{-3}$

Altitude (km)	v_{esc}^{Kep} (m/s)	$v_{esc}^{J_2}$ (m/s)	$v_{esc}^{J_2} - v_{esc}^{Kep}$ (m/s)	$\left\lvert v_{esc}^{J_2} - v_{esc}^{Kep} \right\rvert$ (%)
0	11179.86	11182.88	3.02	0.027
700	10612.65	10614.98	2.33	0.021
1000	10394.65	10396.76	2.10	0.020
5000	8370.43	8371.15	0.71	0.008
10000	6976.72	6977.01	0.28	0.004
40000	4145.98	4146.00	0.02	<0.001

Table 2 Comparison of escape velocities (Keplerian versus J_2 central), Venus; $r_{eq} = 6051 \cdot 10^3$ m; $\mu = 3.249 \cdot 10^{14}$ m^3/s^2; $J_2 = 4.458 \cdot 10^{-6}$

Altitude (km)	v_{esc}^{Kep} (m/s)	v_{esc}^{J2} (m/s)	$v_{esc}^{J_2} - v_{esc}^{Kep}$ (m/s)	$\left\lvert v_{esc}^{J_2} - v_{esc}^{Kep} \right\rvert$ (%)
0	10362.77	10374.32	11.54	0.110
700	9810.83	9819.61	8.78	0.089
1000	9599.85	9607.72	7.87	0.082
5000	7668.12	7670.68	2.56	0.033
10000	6362.66	6363.66	1.00	0.015
40000	3756.38	3756.45	0.07	0.001

Table 3 Comparison of escape velocities (Keplerian versus J_2 central), Jupiter; $r_{eq} = 71492 \cdot 10^3$ m; $\mu = 1.268 \cdot 10^{17}$ m^3/s^2; $J_2 = 0.01475$

Altitude (km)	v_{esc}^{Kep} (m/s)	$v_{esc}^{J_2}$ (m/s)	$v_{esc}^{J_2} - v_{esc}^{Kep}$ (m/s)	$\left\lvert v_{esc}^{J_2} - v_{esc}^{Kep} \right\rvert$ (%)
0	59558.79	59778.01	219.21	0.368
700	59269.33	59483.29	213.95	0.361
1000	59146.57	59358.32	211.74	0.358
5000	57579.33	57764.50	185.17	0.321
10000	55784.96	55943.05	158.09	0.283
40000	47692.79	47765.05	72.25	0.151
540000	20364.75	20365.78	1.02	0.005

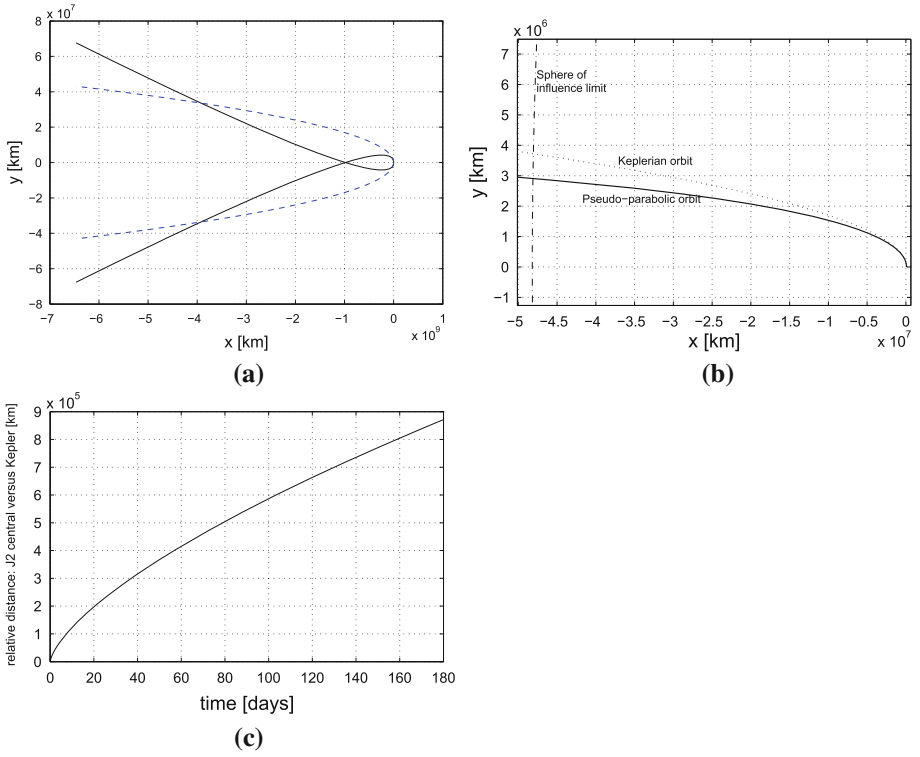

Fig. 8 The fish orbit compared to the Keplerian parabola. **a** A general view. **b** A magnified view inside the sphere of influence. **c** Time variation of the distance between the spacecraft real position and the Keplerian reference

5.1.2 Difference between the Keplerian and the J_2 central models

Figure 8a depicts the difference between the Keplerian parabola and the pseudo-parabolic ("fish") orbit. The orbits are about Jupiter, and they have the same pericenter distance, at an altitude of 500 km above the planet's surface. The loop of the "fish" orbit closes at the distance of 985, 069, 794 km from the attraction center.

5.1.3 Distance between the Keplerian and the J_2 central orbits

The following scenario is analyzed: A spacecraft is injected into a zero-energy orbit from the pericenter, in the equatorial plane, under the effect of J_2. Consider the same spacecraft (the Keplerian reference) which is injected under the same initial conditions, but the J_2 zonal harmonic is not taken into account. The motion of the spacecraft (the real one and its Keplerian reference) is analyzed from the injection moment until the limit of the sphere of influence (SOI) of the planet is reached; the SOI radius is computed as:

$$r_{SOI}^{planet} = a_S \left(\frac{m_{planet}}{M_{Sun}} \right)^{2/5}, \tag{109}$$

where a_S is the planets's heliocentric semimajor axis, m_{planet} is the mass of the planet and M_{Sun} is the mass of the Sun. The same value of 500 km of pericenter distance is used, and both orbits are about Jupiter. The radius of the sphere of influence is $r_{SOI}^{Jupiter} = 48,204,809.19$ km.

Figure 8b depicts the orbit of the spacecraft and its Keplerian reference with respect to the (common) perifocal frame, in the plane of motion. There exist a significant difference between the positions on the two orbits, which reaches values of $9 \cdot 10^5$ km when the SOI limit is reached. Figure 8c depicts the variation of the distance between the spacecraft and its reference with respect to time, from the moment of the launch until reaching the sphere of influence. It may be seen that the difference starts increasing rapidly, and the increase rate decreases as the spacecraft gets further away. However, for the aforementioned initial conditions, the distance between the (real) J_2 central orbit position and its Keplerian counterpart is approximately $2 \cdot 10^5$ km after three weeks from the injection moment.

5.2 Pseudo-hyperbolic orbits

5.2.1 Differences between Flyby models

The examples presented here compare some Keplerian and J_2 central characteristics of flybys in the equatorial plane while using the same initial conditions $\mathbf{r}_0$, $\mathbf{v}_0$,. In the situation of approaching from infinity, the design of the J_2 orbit starts from the assumptions made in the Keplerian scenario, namely, for a classical Keplerian flyby, the pericenter distance r_P and the magnitude of the velocity at infinity v_∞ are given. For a J_2 central flyby, the parameters defining the pseudo-hyperbolic orbit will be computed by knowing that this orbit and the Keplerian reference share the same specific total energy and the same angular momentum.

The scenarios to be analyzed are inspired by the data taken from the Cassini orbiter four flybys, which occurred in 1998–2000, two of them about Venus, one about Earth and one about Jupiter.

For the sake of illustration, the spacecraft and the planet are considered to move collinearly before the flyby, with respect to an inertial reference heliocentric frame. The input data will consist of (i) the velocity at infinity v_∞ and (ii) the flyby lowest altitude (assumed to be determined from Keplerian considerations). The pericenter of the J_2 central orbit does not coincide with the Keplerian pericenter.

The algorithm to derive the data for the J_2 central orbit is given in Sect. 4.2.1: Determine $\mathcal{E}$ from Eq. (91), and determine h from:

Table 4 Cassini Orbiter flybys—pericenter distances

	Date	Planet	Flyby altitude (km)	Speed before flyby (km/s)
1.	26 April 1998	Venus	337	37.2
2.	24 June 1999	Venus	598	39.2
3.	18 August 1999	Earth	1166	35.0
4.	30 December 2000	Jupiter	9,721,846	11.6

Table 5 Cassini Orbiter flybys—results:

	δ_{Kep} (deg)	δ_{J_2} (deg)	$\Delta\delta$ (deg)	ϖ (deg)	r_P (km)	$r_{\min}$ (km)	Δr_P (km)	$\lvert\Delta\mathbf{r}_P\rvert$ (km)
1.	132.282	132.149	0.1329	0.066	6388	6376.29	11.70	13.85
2.	94.887	94.799	0.087	0.043	6649	6639.94	9.05	10.39
3.	82.562	82.546	0.015	0.008	7544.16	7542.23	1.92	2.19
4.	117.957	117.957	$1.3 \cdot 10^{-5}$	$6.66 \cdot 10^{-6}$	9,793,338	9,793,334.7	3.29	3.49

Table 6 Jupiter flybys altitudes

		Date	Planet	Flyby altitude (km)
5.	Pioneer 10	December 1973	Jupiter	130, 000
6.	Pioneer 11	January 1975	Jupiter	42, 828
7.	Voyager 2	July 1979	Jupiter	721, 883
8.	Ulysses	February 1992	Jupiter	428, 952

Table 7 Jupiter flybys—results

	v_∞ (km/s)	$\Delta\delta$ (deg)	ϖ (deg)	r_P (km)	$r_{\min}$ (km)	Δr_P (km)	$\lvert\Delta\mathbf{r}_P\rvert$ (km)
Pioneer 10	11.218	0.052	0.026	201,492	201,335.97	156.02	181.44
Pioneer 11	14.894	0.164	0.082	114,320	114,044.5	275.49	320.32
Voyager 2	5.653	0.003	0.001	793,375	793,335.4	39.59	46.05
Ulysses	7.118	0.008	0.004	500,444	500,381.2	62.78	73.00

$$h = r_P v_P = r_P \sqrt{\frac{2\mu}{r_P} + 2\mathcal{E}} = r_P \sqrt{\frac{2\mu}{r_P} + v_\infty^2}. \tag{110}$$

Now, solve the polynomial equation (60) to determine r_*, $r_{\min}$, r_M which are necessary for making all the computations.

The flight data used are given in Tables 4 and 6, while the results are depicted in Tables 5 and 7.

The notations used are: δ_{Kep} = Keplerian deflection angle; δ_{J_2} = J_2 central deflection angle; $\Delta\delta = \delta_{J_2} - \delta_{Kep}$; r_P = Keplerian flyby altitude; $r_{\min}$ = J_2 central flyby altitude;

ϖ = angle between the Keplerian and the J_2 central pericenter lines; $\Delta r_P = r_{Kep} - r_{\min}$; $|\Delta \mathbf{r}_P|$ = distance between the two pericenters.

All the flybys in Tables 6 and 7 are assumed to take place in the equatorial plane of Jupiter, and the Keplerian eccentricity is assumed to be $e_{Kep} = 1.2$, associated with a Keplerian deflection angle $\delta_{Kep} = 112.885$ degrees. The velocity at infinity is computed based on the minimum distance r_P (assumed to be extracted from the Keplerian model) and the above eccentricity, by using the formula:

$$e_{Kep} = 1 + \frac{r_P v_\infty^2}{\mu} \tag{111}$$

The results obtained within Tables 5 and 7 prove that there is a significant difference in the geometry of the orbit between the Keplerian and the J_2 central models. In order to improve the accuracy of the orbit predictions, the central effects of the J_2 zonal harmonic should be embedded within the analytical model of the trajectory, and the way of doing so was comprehensively approached within the current paper.

6 Conclusions

Analytical solutions for the unbounded motion about an oblate spheroidal planet, while taking into account only the J_2 gravitational harmonic, were determined. The solutions to the equations of motion were expressed with the help of elliptic integrals.

The qualitative and quantitative aspects of the motion were analyzed comprehensively. In the zero-energy case, a new fish-shaped orbit was found, and its characteristics were comprehensively analyzed.

The numerical examples have proven that the J_2 zonal harmonic has a marked effect, which manifests itself for low flyby altitudes. The pseudo-hyperbolic solutions revealed noticeable differences in deflection angles and pericenter positions.

One of the main possible advantages of using the present approach in planning missions that comprise flybys is the increased accuracy of the computations, since they are based on analytical solutions.

Acknowledgments This work was partially supported by the Cecilia and Sam Neaman Postdoctoral Fellowship.

References

Abramowitz, M., Stegun, I.A.: Handbook of Mathematical Functions with Formulas, Graphs, and Mathematical Tables. Dover, New York (1964)

Arnold, V.I., Kozlov, V., Neishtadt, A.: Mathematical Aspects of Classical and Celestial Mechanics. 3rd edn. Springer, Berlin (2006)

Battin, R.H.: An Introduction to the Mathematics and Methods of Astrodynamics. AIAA, Reston, VA (1999)

Beletskii, V.V.: Essays on the motion of celestial bodies. Birkhäuser (2001)

Brouwer, D.: Solution of the problem of artificial satellite theory without drag. Astron. J. **64**, 378–397 (1959)

Celletti, A., Negrini, P.: Non-integrability of the problem of motion around an oblate planet. Celest. Mech. Dyn. Astron. **61**, 253–260 (1995)

Cid, R., Lahulla, J.F.: Perturbaciones de corto periodo en el movimiento de un satélite artificial, en función de las variables de hill. Publ. Rev. Acad. Cienc., Zaragoza **24**, 159–165 (1969)

Coppola, V., Palacián, J.: Elimination of the latitude in artificial satellite theory. J. Astron. Sci. **42**, 27–34 (1994)

Deprit, A., Ferrer, S.: Note on cid's radial intermediary and the method of averaging. Celest. Mech. **40**, 335–343 (1987)

Deprit, A., Ferrer, S.: Simplifications in the theory of artificial satellites. J. Astron. Sci. **37**, 451–463 (1989)
Deprit, A., Rom, A.: The main problem of artificial satellite theory for small and moderate eccentricities. Celest. Mech. **2**(2), 166–206 (1970)
Irigoyen, M., Simo, C.: Nonintegrability of the J_2 problem. Celest. Mech. Dyn. Astron. **55**, 281–287 (1993)
Jezewski, D.J.: An analytic solution for the J_2 perturbed equatorial orbit. Celest. Mech. **30**, 363–371 (1983). doi:10.1007/BF01375506
Kozai, Y.: Second-order solution of artificial satellite theory without air drag. Astron. J. **67**(7), 446–461 (1962)
Lang, T.: Spheroidal Solution for Unbounded Orbits About an Oblate Planet. Master's thesis, Massachusetts Institute of Technology (1968)
Martinusi, V., Gurfil, P.: Solutions and periodicity of satellite relative motion under even zonal harmonics perturbations. Celest. Mech. Dyn. Astron. **111**(4), 387–414 (2011)
O'Mathuna, D.: Satellite prediction formulae for Vinti's model. Celest. Mech. **1**(3-4), 467–478 (1970)
Vallado, D.A.: Fundamentals of Astrodynamics and Applications. Microcosm (2nd edn., 2001)
Vinti, J.: New method of solution for unretarded satellite orbits. J. Res. Nat. Bureau Stand. B Math. Math. Phys. **62**(2), 105–116 (1959)
Vinti, J.: Intermediary equatorial orbits of an artificial satellite. J. Res. Nat. Bureau Stand. B Math. Math. Phys. **66**(1), 5–14 (1961)
Vinti, J.: Intermediary equatorial orbits of an artificial satellite. J. Res. Nat. Bureau Stand. B Math. Math. Phys. **66**(1), 5–14 (1961)
Vinti, J.: Theory of an accurate intermediary orbit for satellite astronomy. J. Res. Nat. Bureau Stand. B Math. Math. Phys. **65**(3), 169–201 (1961)
Vinti, J.P.: Theory of the orbit of an artificial satellite with use of spheroidal coordinates. Astron. J. **65**, 353–354 (1960)
Whitman, P., Matese, J.: Generalized Lagrangian orbital elements for central force problems. Celest. Mech. **36**, 71–82 (1985)